ADVANCED FUNCTIONAL MATERIALS
www.afm-journal.de

www.MaterialsViews.com

Nanoscale Insight Into Lead-Free BNT-BT-*x*KNN

*Robert Dittmer, Wook Jo, Jürgen Rödel, Sergei Kalinin, and Nina Balke**

Piezoresponse force microscopy (PFM) is used to afford insight into the nanoscale electromechanical behavior of lead-free piezoceramics. Materials based on $Bi_{1/2}Na_{1/2}TiO_3$ exhibit high strains mediated by a field-induced phase transition. Using the band excitation technique the initial domain morphology, the poling behavior, the switching behavior, and the time-dependent phase stability in the pseudo-ternary system (1–*x*)(0.94$Bi_{1/2}Na_{1/2}TiO_3$-0.06$BaTiO_3$)-*x*$K_{0.5}Na_{0.5}NbO_3$ (0 <= *x* <= 18 mol%) are revealed. In the base material (*x* = 0 mol%), macroscopic domains and ferroelectric switching can be induced from the initial relaxor state with sufficiently high electric field, yielding large macroscopic remanent strain and polarization. The addition of KNN increases the threshold field required to induce long range order and decreases the stability thereof. For *x* = 3 mol% the field-induced domains relax completely, which is also reflected in zero macroscopic remanence. Eventually, no long range order can be induced for *x* >= 3 mol%. This PFM study provides a novel perspective on the interplay between macroscopic and nanoscopic material properties in bulk lead-free piezoceramics.

1. Introduction

Piezoelectric materials[1] have become an integral part of today's technology in a multitude of devices such as sensors,[2,3] actuators,[4,5] generators,[6,7] and ultrasound transducers.[8–10] Due to their excellent electromechanical properties, lead-zirconate-titanate $PbZr_xTi_{(1-x)}O_3$ (PZT)[11–13] and other lead-containing materials such as $Pb_{(1-y)}La_y$ $(Zr_xTi_{(1-x)})O_3$ (PLZT),[14,15] and (1–*x*) $Pb(Mg_{1/3}Nb_{2/3})O_3$–*x*$PbTiO_3$ (PMN-PT)[16,17] are often the materials of choice.[18] However, the reduction of lead and other hazardous materials from electronics and other consumer products has been sought due to environmental and health concerns.[19] Therefore, international regulations like RoHS[20] and WEEE[21] limit the use of these materials and encourage research for viable substitutes. Despite extensive search, few materials have been discovered that could replace the ubiquitous PZT in the whole spectrum of its applications.[22,23]

A currently emerging competitor to PZT is the pseudobinary system between rhombohedral or monoclinic $Bi_{1/2}Na_{1/2}TiO_3$ (BNT)[24–26] and tetragonal $BaTiO_3$ (BT).[27,28] BNT-*x*BT delivers a comparably high strain and has been studied intensively.[29–31] Similar to PZT, the electromechanical properties are known to be enhanced at the morphotropic phase boundary (MPB) at $x \approx 6$–7 mol%. Interestingly, carefully performed structural studies revealed nothing but a cubic symmetry for compositions near the MPB in their virgin state.[32,33] The crystallographic aspects and their correlation with macroscopic functional properties in this system had remained controversial in the community,[31,34–39] although the average cubic symmetry by diffraction studies was also consistent with the relaxor characteristics suggested by the dielectric permittivity measurement as a function of temperature.[40,41]

Daniels et al.[42] reported on an irreversible, field-induced phase transition in BNT-7BT from the initially pseudocubic to a tetragonal phase on the application of 3 kV mm^{-1}, which was later underpinned by in situ X-ray diffraction study on a series of BNT-BT compositions.[39] A follow-up neutron diffraction measurement further revealed that this field-induced phase transition is accompanied by changes in the oxygen octahedral tilting systems asserting that electric-field application brings about a symmetry change.[43] It is noted that this field-induced change from a pseudocubic to ferroelectric phase from the diffraction point of view is a common feature in relaxor materials.[44–47]

When $K_{0.5}Na_{0.5}NbO_3$ (KNN) is added to BNT-6BT, the remanence in macroscopically measured polarization and strain decays and the ratio of usable strain ΔS to the maximum applied electric field E_{max} is strongly increased (in the following termed d_{33}^*).[33] This strong increase of d_{33}^* is accompanied by a reversible, field-induced phase transition between a pseudocubic and certain non-cubic phases[48] and has drawn great attention from the community. Not only is the phenomenon itself scientifically interesting but it also renders these materials appealing for actuator applications as a replacement for lead-containing materials.

In relaxors and ferroelectrics, the macroscopic polarization and strain are determined by the domain structure and their dynamic response to applied electric fields. In order to identify the origin of the high strains in the materials described above, fundamental knowledge about the domains is needed on the nanoscale level. Piezoresponse force microscopy (PFM) offers a natural pathway for studying electromechanical behavior on the nanoscale and has been widely used to investigate ferroelectric domain structures and local polarization switching in

R. Dittmer, Dr. W. Jo, Prof. J. Rödel
Institute of Materials Science
Technische Universität Darmstadt
Petersenstr. 23, 64287 Darmstadt, Germany
Dr. S. Kalinin, Dr. N. Balke
Functional Imaging on the Nanoscale
Center for Nanophase Materials Sciences
Oak Ridge National Laboratory
M.S. 8610, Oak Ridge, TN 37831
E-mail: balken@ornl.gov

DOI: 10.1002/adfm.201200592

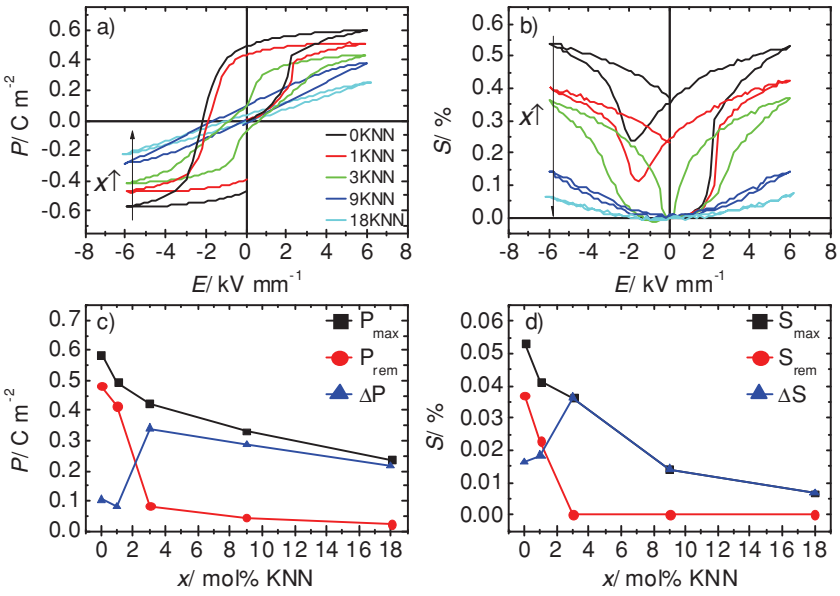

Figure 1. Macroscopic sample properties of a series of BNT-BT-KNN compositions. a) Polarization hysteresis and b) strain hysteresis of the ceramic samples. Extracted values for remanent ($E = 0$) and maximum ($E = 6$ kV mm^{-1}): c) polarization and d) strain.

ferroelectric ceramics, thin films, and capacitors.[47,49–52] Despite the plethora of possibilities that are featured by the PFM technique, it has only rarely been applied to lead-free piezoceramics and was focused with few exceptions[42] on domain imaging in thin films or single crystals.[53–57]

Here, we present a systematic in-depth PFM study of local domain structures, polarization dynamics, and field-induced phase transformations for pseudoternary (1–x)(0.94BNT-0.06BT)-xKNN ceramics with x varying from 0 to 18 mol%. Across this compositional range, the macroscopic material properties, which are drastically altered as shown elsewhere,[58–60] will be compared with the findings of this study. This will provide an understanding of the interplay between macroscopic and nanoscopic material properties. In the following, the samples of different compositions are referred to as xKNN.

2. Results and Discussion

2.1. Macroscopic Properties

The macroscopic properties given in **Figure 1** reflect the well-known behavior that was reported elsewhere.[60]

In 0KNN, the hysteresis loops of the polarization P (Figure 1a) and the strain S (Figure 1b) appear ferroelectric with a coercive field of 2.15 kV mm^{-1}. The strain hysteresis displays typical butterfly shape with very high poling strain S_{pol} of 0.53%. At the same time, it shows a very high remanent strain S_{rem} of 0.35%; therefore, the usable strain ΔS that is repeatedly harvested under unipolar driving conditions is merely 0.18%. With the addition of KNN, the maximum polarization P_{max} and poling strain S_{pol} diminish as noted in Figure 1c,d. At 3 mol% of KNN and above, the remanent polarization P_{rem} drops to a minimum and S_{rem} becomes virtually zero which consequentially leads to a large-strain behavior. With further additions of KNN, ΔS and $d_{33}{}^{*}$ diminish, leaving 3KNN as the composition with the highest strain/field ratio. At the same time, the hysteretic behavior, defined here as the area that is enclosed by the $P(E)$ and $S(E)$ loop, is reduced.

2.2. Domain Imaging

The images from mirror-polished surfaces in **Figure 2** characterize the out-of-plane (OP) and in-plane (IP) PFM amplitudes for all the studied compositions. In 0KNN, there is a very weak OP PFM contrast and virtually no domain-related features are visible. However, the IP polarization component exhibits more variations, revealing a grainy, partly blurry PFM contrast.

The lack of macroscopic domains perfectly underpins the earlier TEM and diffraction studies by different authors who did not observe reflection splittings in unpoled morphotropic BNT-BT.[43,61,62] 1KNN and 3KNN exhbit a more pronounced OP domain contrast with distinguishable grains. 9KNN and 18KNN feature a stronger PFM contrast and, therefore, apparent domains can be distinguished.

2.3. Local Phase Transformations

To explore the possibility of inducing transitions into a ferroelectric phase through electrical fields, local poling experiments were conducted. A negative DC voltage was applied to the tip during scanning of a 3 × 3 μm^2 area. To check for reversibility, a positive voltage of the same amplitude was applied to a 1 × 1 μm^2 area within the poled region.

The OP PFM images after poling with ∓10 V and ∓20 V are presented in **Figure 3**. For 0KNN, a relatively low voltage of 10 V suffices to induce macroscopic domains where the interior square exhibits inverse piezoresponse compared to the external square. This is a clear indication of field-induced ferroelectricity on the microscale (reversible change of remanent polarization) in accordance with the macroscopically measured strain and polarization loops. In contrast, in 1KNN and 3KNN, domains have only partially been induced at 10 V, demonstrated by the dim and incomplete contrast in the electrically excited regions. For 1KNN, an increased voltage of 20 V is sufficient to reversibly pole the material. In 3KNN, on the other hand, 20 V is not sufficient, and in the case of 9KNN and 18KNN domains could not be written even at 20 V. This is consistent with the macroscopic observation of minimum remanent polarization for the latter compositions (Figure 1). Note that the incomplete domain switching for 1KNN and 3KNN is a combined effect of partial switching but also domain relaxation due to the amount of time between poling and imaging. Here we cannot differentiate between these effects but want to emphasize that we compare the poling behavior of the different compositions

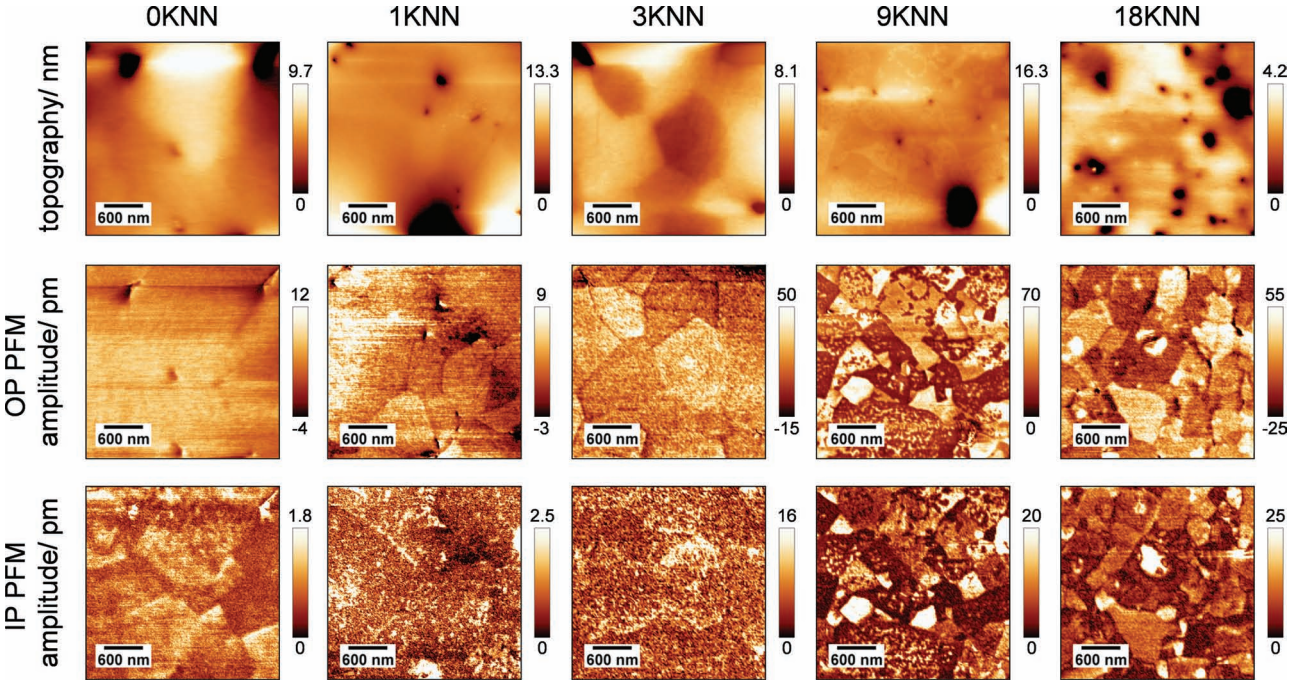

Figure 2. Domain images of unpoled ceramic samples. Topography, OP PFM amplitude, and IP PFM amplitude for *x*KNN.

under the same measurement conditions rendering the differences as sample specific. It is also interesting to note, that the inner squares for 1KNN and 3KNN are more pronounced than the respective outer squares. This observation is likely to be attributed to the doubled duration of field exposure, namely during positive and negative poling, compared to the outer square. Moreover, the poling procedures require that the inner square is poled later than the inner section, which results in

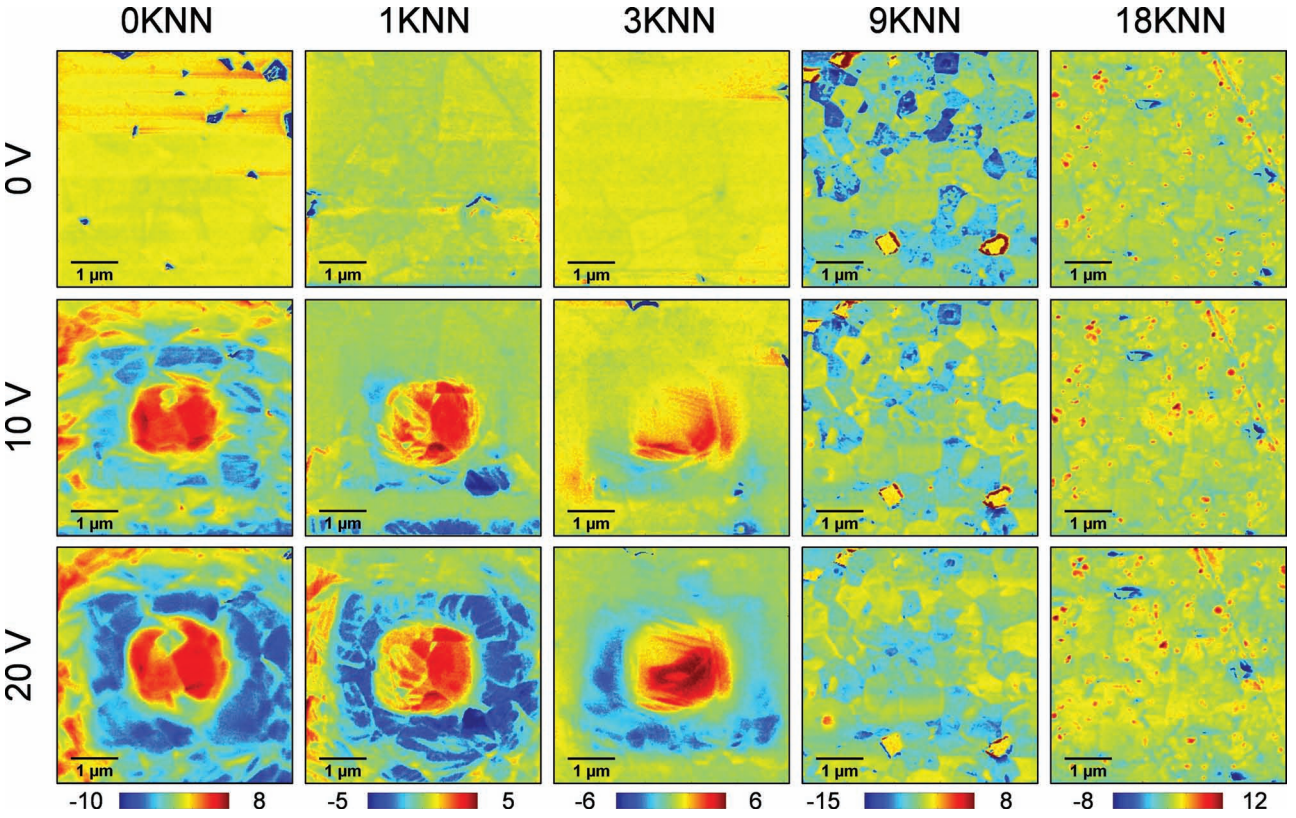

Figure 3. Poling behavior of all compositions. OP PFM images after poling with ∓10 V and ∓20 V in 3×3 µm^2 and 1×1 µm^2, respectively.

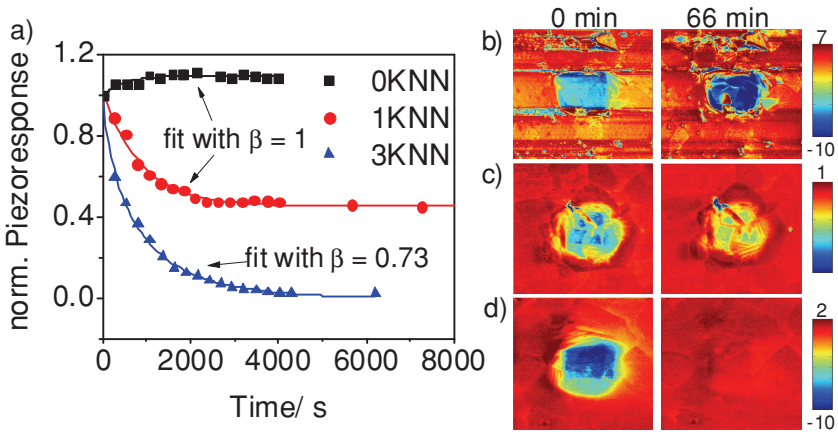

Figure 4. Long-time relaxation measurements using single-frequency PFM. a) Changes of the average PFM signal in the switched area as a function of time. OP PFM images for 3×3 μm^2 areas directly after poling and after 66 min (4000 s) for b) 0KNN, c) 1KNN, and d) 3KNN. The data points for 0KNN and 1KNN for were enhanced due to a tip change, which was accounted for by adding an offset to these data points.

distinct time intervals between poling and final scanning for both areas. As it will be shown in the following, domain relaxation is an important phenomena and must be considered in these materials.

The stability of the switched domain areas was investigated by poling of a 1×1 μm^2 area with –20 V applied to the tip while recording the OP PFM images as a function of time. **Figure 4** provides the relative changes of piezoresponse signal of the scanned region as a function of time for 0KNN, 1KNN, and 3KNN together with the PFM images directly after poling and after approximately 66 min (4000 s). The PFM signal of the switched domains in 0KNN exhibits a slight increase, whereas domains switched in 1KNN display a decrease in PFM signal before asymptotically saturating to a certain value (see Supporting Information for details of PFM amplitude and phase relaxation). The domains switched in 3KNN relaxed fast to zero and were no longer detectable after approximately 2000 s demonstrating reversibility of the field-induced ferroelectric phase. The average PFM signals from the switched domains were fitted using a stretched exponential function in the form of $y_0 + y_1\exp(-t/\tau)\beta$, which is a generally accepted standard function to fit domain relaxation.[63,64] Here, y_0 and y_1 are fitting coefficients to describe offsets as well as signal increase and decrease, and τ and β describe the relaxation time and the stretching exponent, respectively. It was found that the domain relaxation in 0KNN and 1KNN can be described with a single exponential decay ($\beta = 1$), whereas 3KNN is best fitted with $\beta = 0.73 \pm 0.03$. The fitting parameters are given in **Table 1**.

To characterize the nanoscopic ferroelectric switching behavior, piezoresponse loops of individual points were obtained using band excitation (BE) PFM voltage spectroscopy.[65,66] Piezoresponse loops were measured on a 10×10 grid in a 5×5 μm^2 square with the averaged hysteresis loops displayed in **Figure 5** for the various KNN contents.

All five compositions exhibit closed and squared piezoresponse loops. However, there are significant differences in switching behavior. The loops broaden with increasing KNN-content as the switching voltage increases. The coercive voltage U_c was extracted after fitting the ferroelectric loops and is depicted in **Figure 6**. While U_c for 0KNN is 3.5 V, it almost linearly increases to 5.3 V and 8.4 V for 1KNN and 3KNN, respectively. For 9KNN, U_c rises to a very high value of 23.3 V and in 18KNN to an even larger value of 27.4 V. Comparison with macroscopic hysteresis loops (Figure 1) suggests that ferroelectric switching can be induced at sufficiently high fields even in compositions with higher KNN-content. In contrast, an electric field of 6 kV mm^{-1} for the macroscopic measurements did not suffice to induce the ferroelectric phase for >3 mol% KNN. Due to the difficulties in determining quantitative values for the applied electric field in SPM-type experiments, it is not possible to directly conclude the theoretical macroscopic threshold field from the local switching voltage. However, judging from 0KNN with a switching voltage of about 3.5 V and a macroscopic threshold field of 2.25 kV mm^{-1}, the estimated macroscopic switching field for 9KNN and 18KNN

Table 1. Parameters y_0, y_1, β, and τ with the according uncertainty determined for long-time relaxation of piezoresponse in 0KNN, 1KNN, and 3KNN.

Composition	y_0	y_1	β	$\Delta\beta$	τ	$\Delta\tau$
0KNN	1.1	–0.1	1	0.45	491	153
1KNN	0.46	0.55	1	0.1	872	63
3KNN	0	1	0.73	0.03	741	31

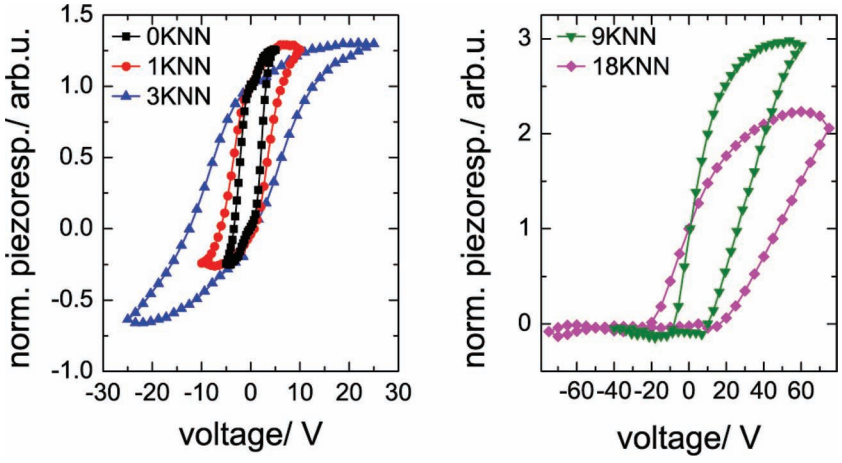

Figure 5. Microscopic piezoresponse hysteresis loops. Locally measured piezoresponse hysteresis loops for different KNN contents for a) 0KNN, 1KNN, and 3KNN and b) 9KNN and 18KNN; averaged over 100 loops from a 5×5 μm^2 area.

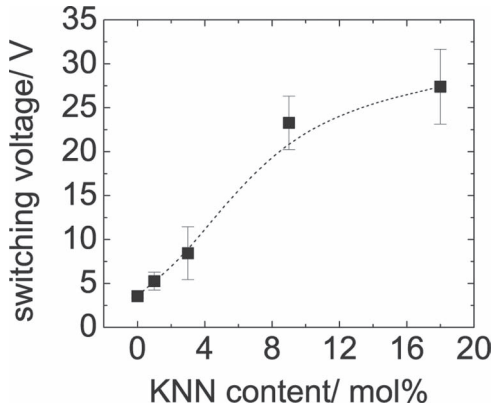

Figure 6. Switching voltage determined from the averaged piezoresponse loops.

may easily exceed 15 kV mm^{-1}. Electric fields this high are not accessible for bulk samples with their high probed volume as the breakdown field is significantly reduced due to the increased probability of finding critical defects. Hence, no or only little switching can be observed in the macroscopic $P(E)$ and $S(E)$ loops of 3KNN, 9KNN, and 18KNN.

To investigate the spatial variation of switching parameters in the individual grains, high-density maps were measured. Here, we performed PFM voltage spectroscopy for 70 × 70 points in an area of 5 × 5 μm^2. The high voltages required to induce switching in 9KNN and 18KNN drastically decreased the lifetime of the tip. Therefore, high-density switching maps were only determined for 0KNN, 1KNN, and 3KNN. The maps for the switching polarization P_{sw} (defined by the loop opening of the piezoresponse loops at zero field) in **Figure 7** display homogeneous P_{sw} within each individual grain but differences from grain to grain. Therefore, the maps of P_{sw} provide a microstructural contrast that resembles topographical maps of thermally or chemically etched microscopy images. This variation can be explained by anisotropic volume change upon ferroelectric switching and randomly distributed grain orientations.

3. Discussion

The lack of macroscopic domains in the virgin state for no or low KNN contents as presented in Figure 2 supports the findings that this compositional series belongs to relaxor ferroelectrics, i.e., there is no apparent long-range order. The lack of clear contrast suggests that there may be polar nanoregions (PNRs) as evidenced by dielectric response.[67] This observation states that the currently investigated materials differ from classical relaxors which often exhibit distinct nanosized domain structures as in PLZT (labyrinthine PNRs, 50 nm),[68] PMN-PT (nanodomains embedded in micrometer-sized domains, 10^0 to 10^2 nm),[69] $Pb(Zn_{1/3}Nb_{2/3})O_3$-4.5 mol%$PbTiO_3$ (PZN-PT, irregular nanodomains, 20–100 nm),[70] or $Sr_{0.61-x}Ba_{0.39}Nb_2O_6:Ce_x^{3+}$ (SBN:Ce, fractal-like nanodomains).[71] However, for PMN single crystals Shvartsman et al.[72] found that most of the surface lacks piezoelectric activity below a threshold voltage. The absence of contrast was rationalized with the small size of the polar clusters from 5 nm to 10 nm. In analogy, we propose that in our experiment the PNRs in 0KNN, 1KNN and 3KNN have sizes that lie below the resolution limit of the PFM measurements and therefore are only pictured as a grainy contrast that is mainly apparent from the in-plane measurements. This finding is in good agreement with earlier TEM measurements where no observable domain contrast[60] or nanodomains[73] were observed and with recent diffuse scattering experiments on BNT-4BT, where a minimum correlation length of 20 nm was determined.[74]

Across the compositional range, ferroelectric phases, i.e., the phases with a long-range order, can be induced when nanoscale volumes are probed as demonstrated in Figure 5. In 0KNN, the required field to induce a long-range order on the nanoscale is comparably small as verified in Figure 6. The addition of small quantities of KNN effectively increases the critical field E_c that is required for this transition. We conclude that critical fields are not reached during the macroscopic measurements in Figure 1, leading to the observed loop distortion for $x \geq 3$ mol% KNN contents.

Long-term relaxation measurements probe the degree of reversibility for the field-induced ferroelectric phase as a function of KNN content. The initially nonergodic relaxor 0KNN is transformed into a long-range-ordered ferroelectric state. Furthermore, the switched ferroelectric phase seems to be stabilized further, indicated by the slight increase in PFM signal over time (see Figure 4a). The underlying reason for this observation is yet to be determined and at this point, we can only conjecture on the physical cause. Firstly, it is possible that internal fields can increase (or decrease) the strength of the measured PFM signal over time. Also, the internal stress state may have altered with time and/or scans. For ferroelectrics like PZT, it is known that d_{33} depends significantly on stress and d_{33} may increase with both increasing and decreasing stress, depending on the initial stress level.[75] To fully clarify the origin of the time-dependent increase of the piezoresponse in 0KNN, further experimental evidence is required.

In 1KNN, the ferroelectric phase can be induced and is stable after an initial relaxation process. Lehnen et al.[71] reported the same effect in the uniaxial relaxor SBN:Ce where relaxation into a "quasistatic" domain was encountered after 4 × 10^4 s, which was rationalized by a microscopical backswitching mechanism. The time-dependence of the

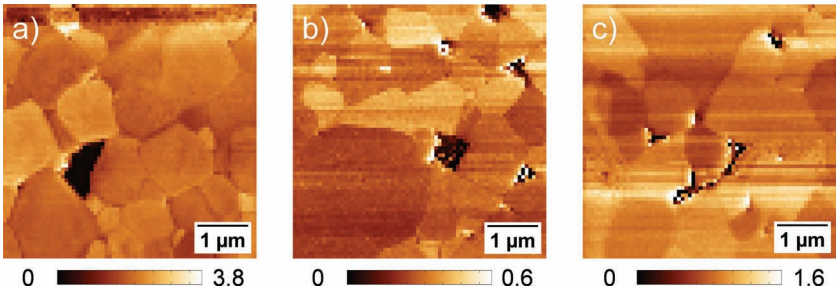

Figure 7. Spatially resolved variations of switching polarization P_{sw} in a 5 × 5 μm^2 area for a) 0KNN, b) 1KNN, and c) 3KNN.

piezoresponse in Figure 4 suggests that backswitching may occur likewise in 1KNN. It is to note that the domains written by means of a DC bias field are spatially limited to the volume close to the sample surface. As the field strength decreases in further distance to the tip,[76] the required threshold field for inducing domains is only reached within a thin near-surface layer. According to Lehnen et al.[71] backswitching in SBN:Ce occurs predominantly at the interface between the induced superficial macrodomain and the adjacent PNRs with two possible mechanisms. These are either depolarization as a consequence of stray fields emerging from the written domain or the formation of nanodomains due to random fields. In contrast, the time-dependent decay of piezoresponse in PLZT reportedly occurs uniformly within the switched area and not by lateral contraction of this area.[47] Close inspection of the time-dependent phase-maps of 1KNN (Supporting Information Figure 1) reveals that the switched area in 1KNN is virtually constant within the inspected time frame. Therefore, the depolarization apparently occurs uniformly across the switched area like in PLZT.

For 3KNN, the switched domains relax quickly back to the initial domain state, i.e., the ferroelectric phase transition is fully reversible and thus the material returns to its initial state. For 9KNN and 18KNN, domain switching cannot be imaged, suggesting an even faster relaxation or insufficient switching fields. Within the limits of the maximum applicable tip voltage of 40 V, no induced domains could be observed. Moreover, the degree of reversibility agrees with the macroscopic measurements of the remanent strain in Figure 1d. Recently, Han et al.[77] reported a possible coexistence of ergodicity and nonergodicity in $LaFeO_3$-modified $Bi_{1/2}(Na_{0.78}K_{0.22})_{1/2}TiO_3$. We suggest that the same mechanism may also hold true for the BNT-BT-based materials. 0KNN is a predominantly nonergodic relaxor that can be converted rather easily into a long-range-ordered state by means of comparatively low electric fields. The introduction of KNN gives rise to an enhancement of random fields resulting from compositional and charge disorder. The volume fraction of ergodic phase increases for 1KNN which leads to the observed partial relaxation of the piezoresponse. Eventually, 3KNN is ergodic to a great extent and therefore the established ferroelectric long-range order collapses at zero field, yielding the high accessible macroscopic strains.[58] At the same time, the threshold value required to establish ferroelectric long-range order increases with KNN content as evidenced in Figure 3. This correlates with the increased switching voltages in Figure 5,6. This finding underpins the hypothesis of enhanced ergodicity.

Judging from the decay of piezoresponse in Figure 4, the accessible strain ΔS and P_{max} should be time-dependent owing to the involved kinetics of relaxation. In a comparable lead-free material system, this time-dependence was indeed confirmed with S_{max} increasing drastically at low frequencies.[78] The time-dependence of macroscopic strain strongly supports the assumption of coexisting ergodicity and nonergodicity.

The domain-like contrast found in 9KNN and 18KNN is in variance with the large-signal measurements where little to no hysteresis was observed asserting virtually no contribution from domains. Also, transmission electron microscopy as well as neutron and X-ray diffraction (not shown) did not provide any indication for the presence of domains in 18KNN. Since diffraction techniques probe an extended bulk volume, the observed contrast might be due to a surface related effect. Without further experimental evidence, we can only conjecture on the nature of this effect. In the case of the ergodic relaxor PMN-0.1PT, it was found that static and dynamic domains exist at the surface while X-ray diffraction yields cubic symmetry.[79] A piezoelectric contrast was also measured on nominally nonpolar $SrTiO_3$,[80] where the surface piezoelectricity was rationalized with the flexoelectric effect.[81,82] A theoretical study by Morozovska et al.[83] later on demonstrated that the local electromechanical response of the nonpiezoelectric $SrTiO_3$ system depends on a plethora of distinct contributions on the nanoscale: Surface electrochemical reactivity may give the same polarity as electromechanical response, yielding a PFM-like signal[84,85] without the presence of actual domains.

In conclusion, the high strain/field ratio rendering 3KNN appealing for actuator applications is afforded by inducing a ferroelectric phase with low bias field below the dielectric breakdown field of the probed sample. At the same time, this transition is reversible and relaxes over time, leading to high S_{max} and low S_{rem}, and thus to high usable strain ΔS.

4. Conclusions

We have presented a comprehensive compositional study on the lead-free BNT-BT-KNN system using piezoresponse force microscopy. By varying the KNN-content from 0 to 18 mol% the macroscopic large-field properties are drastically altered from a ferroelectric characteristic to a relaxor behavior. Using PFM to probe local electromechanical properties, insight into the essential mechanisms on the nanoscale is gained and correlated to macroscopic properties. It was demonstrated that the critical bias field for the relaxor to ferroelectric phase transition is strongly increased with increasing KNN content. These critical fields cannot be accessed with the macroscopic measurements for $x >= 3$ mol% due to larger probing volumes, effectively decreasing breakdown fields. With increasing KNN content, compositional and charge disorder are increased and thus random fields are enhanced. For no or little KNN content, an applied electric field is able to overcome these random fields and establish a long-range order whereas for high KNN contents no such long-range order can be created. It is these random fields which result in a partial or complete relaxation of the piezoelectric response in 1KNN and 3KNN, respectively, after poling.

5. Experimental Section

Materials: Bulk samples of the composition $(1-x)$(0.94BNT-0.06BT)-xKNN (x = 0; 1 mol%; 3 mol%; 9 mol%; 18 mol%) were produced by means of a mixed oxide route. The oxides or carbonates (all Alfa Aesar GmbH & Co. KG, Karlsruhe, Germany) of the respective elements, namely Bi_2O_3 (99.975% purity), Na_2CO_3 (99.5%), K_2CO_3 (99.0%), $BaCO_3$ (99.8%), TiO_2 (99.6%), and Nb_2O_5 (99.9%), were mixed according to their stoichiometric formula and ball-milled in ethanol for 24 h. After drying and subsequent calcination at 900 °C for 3 h, the powders were ball-milled again for 24 h. The dried and sieved powders were uniaxially pressed into pellets of 10 mm diameter. Further compaction was achieved using a cold isostatic press at 300 MPa. Sintering was

carried out at 1100 °C for 3 h in a covered alumina crucible. To minimize evaporation of volatile elements, the pellets were covered in atmospheric powder of the respective composition.

For the macroscopic electrical characterization, pellets were ground down to 1 mm height and painted with silver paste that was burnt in afterwards at 400 °C to form the electrodes.

For the PFM observations the sintered samples were ground down to about 250 µm and subsequently polished using polycrystalline diamond paste with abrasive particles of 15 µm, 6 µm, 3 µm, 1 µm, and 0.25 µm (DP-Paste P by Struers A/S, Ballerup, Denmark) for 1 h each. The finishing was done in a last polishing step of 15 min with a colloidal silica polishing suspension (Buehler Mastermet by Buehler GmbH, Düsseldorf, Germany).

Methods: The small and large field properties were acquired by means of a Sawyer-Tower setup with an optical sensor (Philtec, Inc., Annapolis, Maryland). The setup is described in detail elsewhere.[86]

The PFM experiments were carried out on a MFP-3D and a Cypher AFM (Asylum Research, Santa Barbara, California) using Pt/Ir coated conductive tips (Nanosensors, Neuchatel, Switzerland). For the microscopic piezoelectric response loops a grid of 10×10 points in an area of 5×5 µm^2 was scanned with an AC voltage of 2 V with varying maximum bias fields. The applied technique of band excitation (BE) voltage spectroscopy is described in detail elsewhere.[66] For 0KNN, 1KNN and 3KNN d_{33}-loops were additionally measured using a dense grid of 70×70 points in an area of 5×5 µm^2.

Supporting Information

Supporting Information is available from the Wiley Online Library or from the author.

Acknowledgements

This research was conducted at the Center for Nanophase Materials Sciences, which is sponsored at the Oak Ridge National Laboratory by the Scientific User Facilities Division, Office of Basic Energy Sciences, U.S. Department of Energy. R.D. acknowledges support from the Deutsche Forschungsgemeinschaft (DFG) under SFB595 and from Deutscher Akademischer Austausch Dienst (DAAD) through a stipend for Ph.D. research studies.

Received: February 29, 2012
Revised: May 10, 2012
Published online: June 13, 2012

[1] G. H. Haertling, *J. Am. Ceram. Soc.* **1999**, *82*, 797.
[2] J. F. Tressler, S. Alkoy, R. E. Newnham, *J. Electroceram.* **1998**, *2*, 257.
[3] C. H. Keilers, F. K. Chang, *J. Intell. Mater. Syst. Struct.* **1995**, *6*, 649.
[4] Y. Sugawara, K. Onitsuka, S. Yoshikawa, Q. C. Xu, R. E. Newnham, K. Uchino, *J. Am. Ceram. Soc.* **1992**, *75*, 996.
[5] H. Adriaens, W. L. de Koning, R. Banning, *IEEE-ASME Trans. Mechatron.* **2000**, *5*, 331.
[6] S. R. Anton, H. A. Sodano, *Smart Mater. Struct.* **2007**, *16*, R1.
[7] T. Rödig, A. Schönecker, G. Gerlach, *J. Am. Ceram. Soc.* **2010**, *93*, 901.
[8] W. A. Smith, B. A. Auld, *IEEE Trans. Ultrason. Ferroelectr. Freq. Control* **1991**, *38*, 40.
[9] S. E. Park, T. R. Shrout, *IEEE Trans. Ultrason. Ferroelectr. Freq. Control* **1997**, *44*, 1140.
[10] K. Uchino, *Piezoelectric Actuators and Ultrasonic Motors*, Springer-Verlag GmbH, Heidelberg **1996**.
[11] R. Guo, L. E. Cross, S. E. Park, B. Noheda, D. E. Cox, G. Shirane, *Phys. Rev. Lett.* **2000**, *84*, 5423.
[12] B. Jaffe, R. S. Roth, S. Marzullo, *J. Appl. Phys.* **1954**, *25*, 809.
[13] H. Jaffe, *J. Am. Ceram. Soc.* **1958**, *41*, 494.
[14] G. H. Haertling, C. E. Land, *J. Am. Ceram. Soc.* **1971**, *54*, 1.
[15] S. T. Liu, J. D. Heaps, O. N. Tufte, *IEEE Trans. Sonics Ultrason.* **1972**, *19*, 281.
[16] S. E. Park, T. R. Shrout, *Mater. Res. Innov.* **1997**, *1*, 20.
[17] S. J. Jang, K. Uchino, S. Nomura, L. E. Cross, *Ferroelectrics* **1980**, *27*, 31.
[18] D. Damjanovic, *Rep. Prog. Phys.* **1998**, *61*, 1267.
[19] P. K. Panda, *J. Mater. Sci.* **2009**, *44*, 5049.
[20] The European Parliament and the Council of the European Union, *Off. J. Eur. Union* **2003**, *46*, 19.
[21] The European Parliament and the Council of the European Union, *Off. J. Eur. Union* **2003**, *46*, 24.
[22] T. R. Shrout, S. J. Zhang, *J. Electroceram.* **2007**, *19*, 111.
[23] J. Rödel, W. Jo, K. T. P. Seifert, E. M. Anton, T. Granzow, D. Damjanovic, *J. Am. Ceram. Soc.* **2009**, *92*, 1153.
[24] G. A. Smolenskii, V. A. Isupov, A. I. Agranovskaya, N. N. Krainik, *Sov. Phys. Solid State* **1961**, *2*, 2651.
[25] G. O. Jones, P. A. Thomas, *Acta Crystallogr. Sect. B-Struct. Sci.* **2002**, *58*, 168.
[26] E. Aksel, J. S. Forrester, J. L. Jones, P. A. Thomas, K. Page, M. R. Suchomel, *Appl. Phys. Lett.* **2011**, *98*, 152901.
[27] S. Roberts, *Phys. Rev.* **1947**, *71*, 890.
[28] A. F. Devonshire, *Philos. Mag.* **1949**, *40*, 1040.
[29] S. Trujillo, J. Kreisel, Q. Jiang, J. H. Smith, P. A. Thomas, P. Bouvier, F. Weiss, *J. Phys.: Condens. Matter* **2005**, *17*, 6587.
[30] Y.-M. Chiang, G. W. Farrey, A. N. Soukhojak, *Appl. Phys. Lett.* **1998**, *73*, 3683.
[31] T. Takenaka, K. Maruyama, K. Sakata, *Jpn. J. Appl. Phys. Part 1* **1991**, *30*, 2236.
[32] R. Ranjan, A. Dviwedi, *Solid State Commun.* **2005**, *135*, 394.
[33] S. T. Zhang, A. B. Kounga, E. Aulbach, H. Ehrenberg, J. Rödel, *Appl. Phys. Lett.* **2007**, *91*, 112906.
[34] W. Jo, J. Rödel, *Appl. Phys. Lett.* **2011**, *99*, 042901.
[35] B. Wylie-van Eerd, D. Damjanovic, N. Klein, N. Setter, J. Trodahl, *Phys. Rev. B* **2010**, *82*, 104112.
[36] W. Jo, S. Schaab, E. Sapper, L. A. Schmitt, H.-J. Kleebe, A. J. Bell, J. Rödel, *J. Appl. Phys.* **2011**, *110*, 074106.
[37] J. Wang, Y. Liu, R. L. Withers, A. Studer, Q. Li, L. Norén, Y. Guo, *J. Appl. Phys.* **2011**, *110*, 084114.
[38] X. Tan, C. Ma, J. Frederick, S. Beckman, K. G. Webber, *J. Am. Ceram. Soc.* **2011**, *94*, 4091.
[39] W. Jo, J. E. Daniels, J. L. Jones, X. Tan, P. A. Thomas, D. Damjanovic, J. Rödel, *J. Appl. Phys.* **2011**, *109*, 014110.
[40] S.-T. Zhang, A. B. Kounga, E. Aulbach, Y. Deng, *J. Am. Ceram. Soc.* **2008**, *91*, 3950.
[41] T. Oh, M.-H. Kim, *Mater. Sci. Eng., B* **2006**, *132*, 239.
[42] R. P. Herber, G. A. Schneider, S. Wagner, M. J. Hoffmann, *Appl. Phys. Lett.* **2007**, *90*, 252905.
[43] H. Simons, J. Daniels, W. Jo, R. Dittmer, A. Studer, M. Avdeev, J. Rödel, M. Hoffman, *Appl. Phys. Lett.* **2011**, *98*, 082901.
[44] A. A. Bokov, Z. G. Ye, *J. Mater. Sci.* **2006**, *41*, 31.
[45] G. Schmidt, H. Arndt, G. Borchhardt, J. Voncieminski, T. Petzsche, K. Borman, A. Sternberg, A. Zirnite, V. A. Isupov, *Phys. Status Solidi A* **1981**, *63*, 501.
[46] E. V. Colla, E. Y. Koroleva, N. M. Okuneva, S. B. Vakhrushev, *Phys. Rev. Lett.* **1995**, *74*, 1681.
[47] A. Kholkin, A. Morozovska, D. Kiselev, I. Bdikin, B. Rodriguez, P. P. Wu, A. Bokov, Z. G. Ye, B. Dkhil, L. Q. Chen, M. Kosec, S. V. Kalinin, *Adv. Funct. Mater.* **2011**, *21*, 1977.
[48] M. Hinterstein, M. Knapp, M. Hölzel, W. Jo, A. Cervellino, H. Ehrenberg, H. Fuess, *J. Appl. Cryst.* **2010**, *43*, 1314.
[49] A. Gruverman, O. Auciello, H. Tokumoto, *Annu. Rev. Mater. Sci.* **1998**, *28*, 101.
[50] S. V. Kalinin, D. A. Bonnell, *Phys. Rev. B* **2001**, *63*, 125411.

[51] A. Gruverman, *Appl. Phys. Lett.* **1999**, *75*, 1452.
[52] C. H. Ahn, K. M. Rabe, J.-M. Triscone, *Science* **2004**, *303*, 488.
[53] R. Tiruvalam, A. Kundu, A. Soukhojak, S. Jesse, S. V. Kalinin, *Appl. Phys. Lett.* **2006**, *89*, 112901.
[54] M. Cernea, A. Galca, M. Cioangher, C. Dragoi, G. Ioncea, *J. Mater. Sci.* **2011**, *46*, 5621.
[55] N. Yasuda, S. Otsuka, H. Ohwa, K. Fujita, M. Iwata, H. Terauchi, Y. Ishibashi, *Ferroelectrics* **2011**, *415*, 67.
[56] F. Remondiere, A. Wu, P. M. Vilarinho, J. P. Mercurio, *Appl. Phys. Lett.* **2007**, *90*, 152905.
[57] D. Y. Wang, D. M. Lin, K. S. Wong, K. W. Kwok, J. Y. Dai, H. L. W. Chan, *Appl. Phys. Lett.* **2008**, *92*, 222909.
[58] W. Jo, T. Granzow, E. Aulbach, J. Rödel, D. Damjanovic, *J. Appl. Phys.* **2009**, *105*, 094102.
[59] S. T. Zhang, A. B. Kounga, W. Jo, C. Jamin, K. Seifert, T. Granzow, J. Rödel, D. Damjanovic, *Adv. Mater.* **2009**, *21*, 4716.
[60] S. T. Zhang, A. B. Kounga, E. Aulbach, T. Granzow, W. Jo, H. J. Kleebe, J. Rödel, *J. Appl. Phys.* **2008**, *103*, 034107.
[61] J. E. Daniels, W. Jo, J. Rödel, J. L. Jones, *Appl. Phys. Lett.* **2009**, *95*, 032904.
[62] J. Wang, Y. Liu, R. L. Withers, A. Studer, Q. Li, L. Noren, Y. Guo, *J. Appl. Phys.* **2011**, *110*, 084114.
[63] A. Kholkin, I. Bdikin, D. Kiselev, V. Shvartsman, S. H. Kim, *J. Electroceram.* **2007**, *19*, 83.
[64] D. C. Lupascu, S. Fedosov, C. Verdier, J. Rödel, H. v. Seggern, *J. Appl. Phys.* **2004**, *95*, 1386.
[65] S. Jesse, S. V. Kalinin, R. Proksch, A. P. Baddorf, B. J. Rodriguez, *Nanotechnology* **2007**, *18*, 435503.
[66] S. Jesse, A. P. Baddorf, S. V. Kalinin, *Appl. Phys. Lett.* **2006**, 88, 062908.
[67] W. Jo, S. Schaab, E. Sapper, L. A. Schmitt, H.-J. Kleebe, A. J. Bell, J. Rödel, *J. Appl. Phys.* **2011**, *110*, 074106.
[68] V. V. Shvartsman, A. L. Kholkin, A. Orlova, D. Kiselev, A. A. Bogomolov, A. Sternberg, *Appl. Phys. Lett.* **2005**, *86*, 202907.
[69] V. V. Shvartsman, A. L. Kholkin, *Phys. Rev. B* **2004**, *69*, 014102.
[70] I. K. Bdikin, V. V. Shvartsman, A. L. Kholkin, *Appl. Phys. Lett.* **2003**, *83*, 4232.
[71] P. Lehnen, W. Kleemann, T. Woike, R. Pankrath, *Phys. Rev. B* **2001**, *64*, 224109.
[72] V. V. Shvartsman, A. L. Kholkin, M. Tyunina, J. Levoska, *Appl. Phys. Lett.* **2005**, *86*, 222907.
[73] L. Schmitt, J. Kling, M. Hinterstein, M. Hoelzel, W. Jo, H. J. Kleebe, H. Fuess, *J. Mater. Sci.* **2011**, *46*, 4368.
[74] J. E. Daniels, W. Jo, J. Rödel, D. Rytz, W. Donner, *Appl. Phys. Lett.* **2011**, *98*, 252904.
[75] I. Kerkamm, P. Hiller, T. Granzow, J. Rödel, *Acta Mater.* **2009**, *57*, 77.
[76] H.-J. Ding, P.-F. Hou, F.-L. Guo, *Int. J. Solids Struct.* **2000**, *37*, 3201.
[77] H.-S. Han, W. Jo, J. Rödel, I.-K. Hong, W.-P. Tai, J.-S. Lee, unpublished.
[78] J. A. Armstrong, N. Bloembergen, J. Ducuing, P. S. Pershan, *Phys. Rev.* **1962**, *127*, 1918.
[79] S. V. Kalinin, B. J. Rodriguez, J. D. Budai, S. Jesse, A. N. Morozovska, A. A. Bokov, Z. G. Ye, *Phys. Rev. B* **2010**, *81*, 064107.
[80] A. Kholkin, I. Bdikin, T. Ostapchuk, J. Petzelt, *Appl. Phys. Lett.* **2008**, *93*, 222905.
[81] A. K. Tagantsev, *Phase Transit.* **1991**, *35*, 119.
[82] L. Cross, *J. Mater. Sci.* **2006**, *41*, 53.
[83] A. N. Morozovska, E. A. Eliseev, G. S. Svechnikov, S. V. Kalinin, *Phys. Rev. B* **2011**, *84*, 045402.
[84] A. Kumar, F. Ciucci, A. N. Morozovska, S. V. Kalinin, S. Jesse, *Nat. Chem.* **2011**, *3*, 707.
[85] N. Balke, S. Jesse, A. N. Morozovska, E. Eliseev, D. W. Chung, Y. Kim, L. Adamczyk, R. E. Garcia, N. Dudney, S. V. Kalinin, *Nat. Nanotechnol.* **2010**, *5*, 749.
[86] N. Balke, D. C. Lupascu, T. Granzow, J. Rödel, *J. Am. Ceram. Soc.* **2007**, *90*, 1081.